











# The plasmonic BTO-on-SiN platform – beyond 200 GBd modulation for optical communications

## Journal Article

### Author(s):

Kohli, Manuel; [Chelladurai, Daniel](#) ; [Kulmer, Laurenz](#) ; [Blatter, Tobias](#) ; [Horst, Yannik Matthias Julius](#) ; [Keller, Killian](#) ; [Doderer, Michael](#) ; [Winiger, Joel](#); [Moor, David](#) ; [Messner, Andreas](#) ; [Buriakova, Tatiana](#); [Convertino, Clarissa](#); [Eltes, Felix](#); [Fedoryshyn, Yuriy](#); [Koch, Ueli](#) ; [Leuthold, Juerg](#) 

### Publication date:

2025-12-16

### Permanent link:

<https://doi.org/https://doi.org/10.3929/ethz-c-000790617>

### Rights / license:

[Creative Commons Attribution 4.0 International](#)

### Originally published in:

Light: Science & Applications 14, <https://doi.org/10.1038/s41377-025-02116-1>

### Funding acknowledgement:

- Neuro-augmented 112Gbaud CMOS plasmonic transceiver platform for Intra- and Inter-DCI ()

ARTICLE

Open Access

# The plasmonic BTO-on-SiN platform – beyond 200 GBd modulation for optical communications

Manuel Kohli<sup>1</sup>✉, Daniel Chelladurai<sup>1</sup>, Laurenz Kulmer<sup>1</sup>, Tobias Blatter<sup>1</sup>, Yannik Horst<sup>1</sup>, Killian Keller<sup>1</sup>, Michael Doderer<sup>1</sup>, Joel Winiger<sup>1</sup>, David Moor<sup>1</sup>, Andreas Messner<sup>1</sup>, Tatiana Buriakova<sup>2</sup>, Clarissa Convertino<sup>3</sup>, Felix Eltes<sup>3</sup>, Yuriy Fedoryshyn<sup>1</sup>, Ueli Koch<sup>1</sup> and Juerg Leuthold<sup>1</sup>✉

## Abstract

An integrated photonics platform that offers high-speed modulators in addition to low-loss and versatile passive components is highly sought after for different applications ranging from AI to next-generation Tbit/s links in optical fiber communication. For this purpose, we introduce the plasmonic BTO-on-SiN platform for high-speed electro-optic modulators. This platform combines the advantages provided by low-loss silicon nitride (SiN) photonics with the highly nonlinear barium titanate (BTO) as the active material. Nanoscale plasmonics enables high-speed modulators operating at electro-optical bandwidths up to 110 GHz with active lengths as short as 5  $\mu\text{m}$ . Here, we demonstrate three different modulators: a 256 GBd C-band Mach-Zehnder (MZ) modulator, a 224 GBd C-band IQ modulator – being both the first BTO IQ and the first IQ modulator on SiN for data communication – and finally, a 200 GBd O-band racetrack (RT) modulator. With this approach we show record data rates of 448 Gbit/s with the IQ modulator and 340 Gbit/s with the MZ modulator. Furthermore, we demonstrate the first plasmonic RT modulator with BTO and how it is ideally suited for low complexity communication in the O-band with low device loss of 2 dB. This work leverages the SiN platform and shows the potential of this technology to serve as a solution to combat the ever-increasing demand for fast modulators.

## Introduction

A high-speed photonic platform that offers a combination of electro-optic modulators with low-loss passive components is essential in many fields where light must be manipulated with electrical signals. For instance, such a combination can be crucial to further advance Tbit/s optical communication links<sup>1</sup>, photonic quantum computing<sup>2</sup>, input/output interfaces to cryogenic environments<sup>3–6</sup>, disaggregated AI systems<sup>7</sup>, microwave photonics<sup>8,9</sup>, and optical computing<sup>10,11</sup>. To meet the increased total traffic demands and complexity in systems, the ideal integrated optical platform should offer high speed operation, a compact footprint, enable operation across the largest possible spectral range, and be able to handle high input powers.

There exists a variety of different platforms and approaches for integrated high-speed modulators. An important metric to demonstrate the potential of a technology is the maximum achievable signal bandwidth. Demonstrations over 200 GBd in the C-band include BTO plasmonics with symbol rates up to 216 GBd<sup>12</sup>, POH up to 256 GBd<sup>13</sup>, and TFLN up to 260 GBd<sup>14</sup>. Most of these demonstrations were realized by intensity modulation and direct detection (IM/DD) schemes. Coherent transmission, on the other hand, is ideal for high data rates in long-haul communications, where complex modulation formats with IQ modulators allow the encoding of information in both phase and amplitude of the light. Examples of IQ modulators operating beyond 100 GBd include plasmonic-organic hybrid (POH) experiments showing single-polarization net-data rates of 790 Gbit/s at 160 GBd<sup>15</sup>, silicon photonics with polarization multiplexed (PMUX) net-data rates of 1 Tbit/s at 105 GBd<sup>16</sup>, thin-film lithium niobate (TFLN) with PMUX net-rates of 1.96 Tbit/s at 130 GBd<sup>17</sup>, and InP with PMUX

Correspondence: Manuel Kohli (mkohli@ethz.ch) or Juerg Leuthold (Leuthold@ethz.ch)

<sup>1</sup>ETH Zurich, Institute of Electromagnetic Fields, Zurich, Switzerland

<sup>2</sup>Ligentec SA, Ecublens, Switzerland

Full list of author information is available at the end of the article

© The Author(s) 2025



**Open Access** This article is licensed under a Creative Commons Attribution 4.0 International License, which permits use, sharing, adaptation, distribution and reproduction in any medium or format, as long as you give appropriate credit to the original author(s) and the source, provide a link to the Creative Commons licence, and indicate if changes were made. The images or other third party material in this article are included in the article's Creative Commons licence, unless indicated otherwise in a credit line to the material. If material is not included in the article's Creative Commons licence and your intended use is not permitted by statutory regulation or exceeds the permitted use, you will need to obtain permission directly from the copyright holder. To view a copy of this licence, visit <http://creativecommons.org/licenses/by/4.0/>.

net-rates of 2.03 Tbit/s at 192 GBd<sup>18</sup>. To achieve such high numbers, most demonstrations utilize probabilistic shaping of high-order modulation formats (up to 100QAM and more) in addition to PMUX, where data is encoded on carriers with orthogonal polarization. In contrast, the O-band is ideally suited for low-complexity, and therefore low-cost applications with IM/DD, due to low fiber dispersion<sup>19</sup>. Recently, directly modulated lasers have been demonstrated to achieve 256 GBd in the O-band<sup>20</sup>, which is an attractive option for intra-data center communications. Integrated solutions with high symbol rates include TFLN<sup>21,22</sup> modulators operating at 210 GBd and InP absorption modulators at 256 GBd<sup>23</sup>.

Although impressive demonstrations, high-speed modulators could generally benefit from the advanced passive performance, scalability, ultra-low loss<sup>24,25</sup>, transparency across a large spectral range<sup>26,27</sup>, and the ability to handle high input power due to negligible two-photon absorption and relatively low stimulated Brillouin scattering<sup>28</sup> offered by SiN photonics. Its advantages have brought forward impressive demonstrations such as frequency comb generation<sup>29,30</sup>, on-chip amplifiers<sup>31</sup>, quantum sources<sup>32</sup>, and lasers<sup>33,34</sup>. Yet, SiN does not offer an electro-optic effect to modulate the light at high frequencies. Among all nonlinear effects, the Pockels effects is particularly interesting as it offers a pure phase modulation<sup>35</sup>. Within interferometric configurations, one can also implement amplitude or intensity modulation. With the demonstration of ultra-low losses in TFLN<sup>36</sup>, it has been developed into a highly versatile platform with a Pockels effect for many different applications<sup>37,38</sup>. In contrast to TFLN, however, SiN is CMOS compatible and already available on 300 mm wafers as it can be grown directly on silicon photonics. Therefore, significant effort has been dedicated to integrating Pockels-effect modulators onto the SiN platform. Examples include PZT-based modulators reaching 40 GBd<sup>39</sup>, SiN-loaded TFLN reaching 80 GBd<sup>40,41</sup>, and heterogeneously integrated TFLN reaching 80 GBd<sup>42–45</sup>. SiN loaded BTO has been leveraged to demonstrate ultra-low-power tuning<sup>46</sup>. By utilizing a plasmonic slot waveguide, it is possible to achieve modulation in a most compact footprint and very high speeds. More recently, we introduced plasmonic BTO-on-SiN and demonstrated 216 GBd in the C-band<sup>12</sup>. BTO has emerged as a viable candidate for integrated electro-optic modulators<sup>47–50</sup>. It offers one of the largest Pockels coefficients among known materials<sup>51</sup>, it is suited for cryogenic environments<sup>3</sup>, and allows wafer-scale integration with advanced platforms<sup>2,52</sup>. Furthermore, BTO with the combination of plasmonics offers exceptionally good thermal stability up to 250 °C in addition to longtime stable operation at 90 °C<sup>53</sup>. It is therefore conceivable that the combination of SiN with BTO gives access to a scalable integrated optical platform that offers highest speed

on a compact footprint, with an ability to handle high power across a wide spectrum.

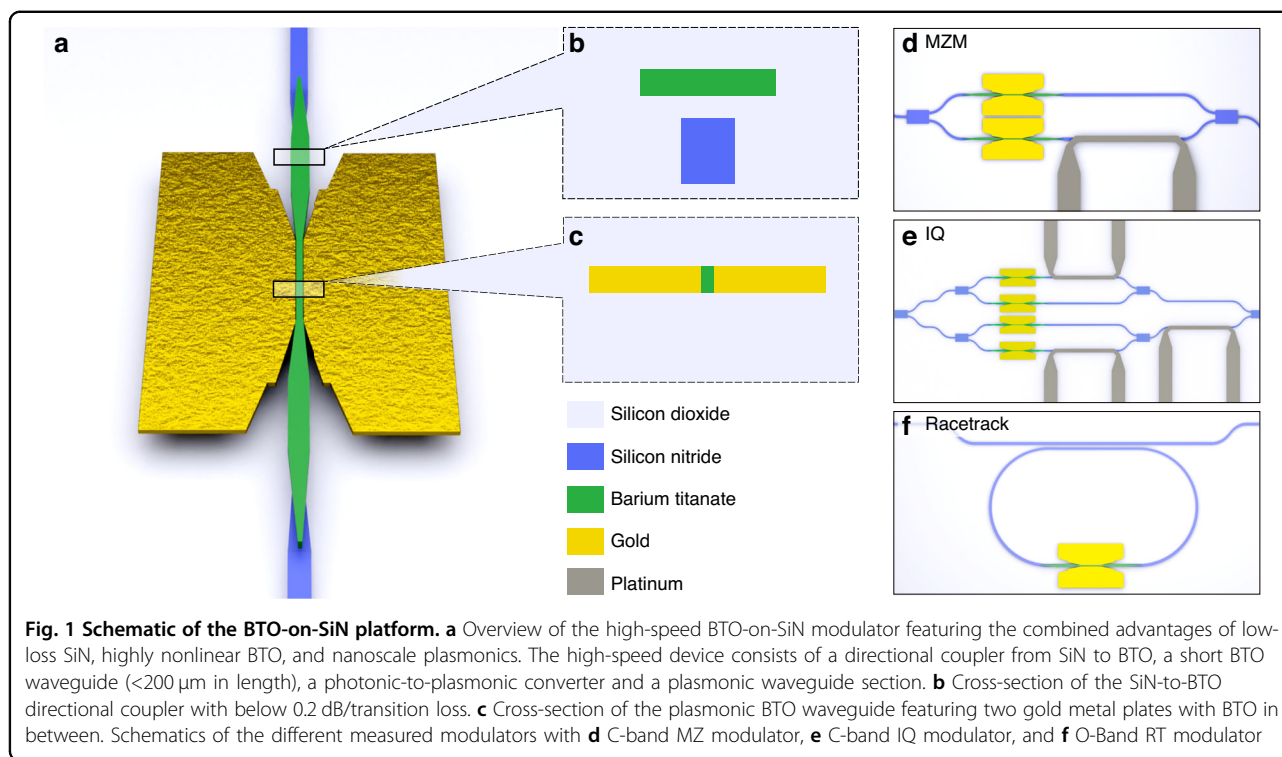
In this work, we show the potential of the BTO-on-SiN integrated optical platform that allows for the implementation of a wide variety of active components targeted for different applications, more specifically short-haul and long-haul communication. For instance, we demonstrate fully integrated Mach-Zehnder (MZ), IQ, and racetrack (RT) modulators. Operation with this BTO-on-SiN platform is shown up to highest speed of 256 GBd and line rates of up to 448 Gbit/s. Such high speed has been enabled by implementing plasmonic metal-insulator-metal active sections that operate up to 110 GHz. The favorable frequency response enables operation with as little as 1.13 V<sub>pp</sub> at 200 GBd – which by any standard makes it an attractive solution for driverless operation. The plasmonic approach further allows integration of the active components on a most compact footprint, which may be as small as 5, 15 and 17.5 μm for the RT, the MZ and the IQ modulators, respectively. This work demonstrates the first BTO-based IQ modulator and the first IQ modulator on SiN. The IQ modulator is the ideal configuration for long-haul communication. The combination of the low loss SiN passive technology with the resonant BTO-plasmonic RT modulators in O-band, ideally suited for low-cost intensity-modulation/direct-detection scheme, yields devices with low 2 dB on-chip losses. Lastly, we show operation across a large spectral window by demonstrating devices for the 1300 and 1550 nm window. All devices were fabricated on the same chip with the same method, and we thus elevate the plasmonic BTO approach to a modulator platform that can be tailored to the specific application. To tackle the energy efficiency required for new optical engines, we demonstrate that high-speed performance of these modulators is achieved even with low-complexity linear offline digital signal processing (DSP), which could enable energy-efficient real-time processing. The plasmonic BTO-on-SiN platform can reach up to 196 GBd with linear equalization only.

The paper is based in part on work that was initially presented at OFC'24 and CLEO'24 conferences<sup>54,55</sup>.

## Results

### BTO-on-SiN platform

The BTO-on-SiN platform aims to combine the advantages provided by the low-loss SiN, the nonlinear BTO with one of the highest Pockels effect among known materials, and the nanoscale plasmonics offering highest speed in most compact configurations. A basic building block of a Pockels modulator is the phase shifter. More complex configurations of modulators, such as the MZ and IQ, can be composed of multiple phase shifters. A schematic of the high-speed plasmonic BTO-on-SiN

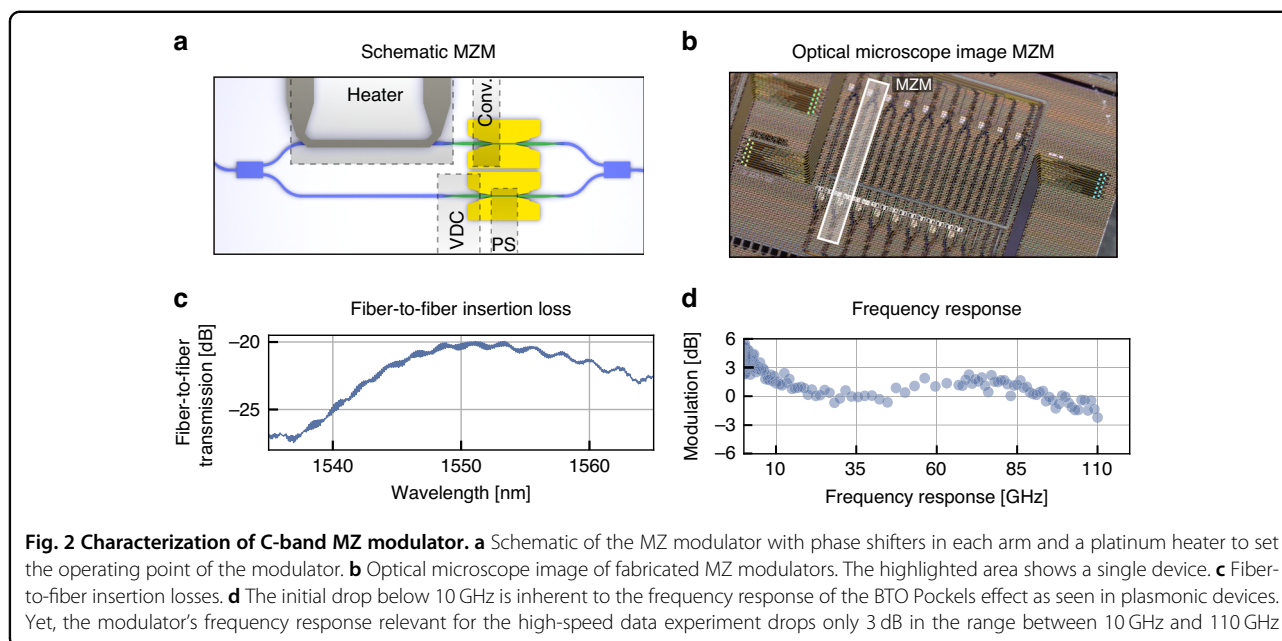


phase shifter, capable of 110 GHz operation, is shown in Fig. 1a. The modulator can be divided into two main parts, the SiN passives used to route the light on the chip, and the phase shifters on the top layers composed of BTO and gold.

The silicon nitride waveguide is fully embedded in SiO<sub>2</sub> and features a cross-section of 800 × 800 nm<sup>2</sup> in the C-band and 600 × 800 nm<sup>2</sup> in the O-band. The fiber-to-chip coupling is solved by employing amorphous silicon overlay grating couplers in a simple scheme. By adding a metallic mirror to the same structure, the coupling efficiency is improved from −2.2 dB to −1.4 dB in experiment and from −1.1 dB to −0.44 dB in simulation<sup>56</sup>. The O-band gratings are designed to be dual-polarization with a high efficiency of −2.5 dB in simulation and −3 dB in experiment for coupling both TE and TM polarizations with the same grating<sup>56</sup>. A heater based on a 100-nm-thick and 2- $\mu\text{m}$ -wide platinum strip can be used to control the phase relation in interferometric configurations such as MZ and IQ modulator. This metal is located ~1  $\mu\text{m}$  above the SiN waveguide separated by SiO<sub>2</sub> cladding. For future improvements in terms of footprint and energy efficiency, the phase tuners could be optimized by increasing the thermal isolation<sup>57</sup>, or replaced for example with solutions based on Pockels effect or on liquid crystals<sup>46,58–60</sup>.

The phase shifters are composed of the following parts: a vertical directional coupler (VDC) to couple the light to the BTO, a photonic-to-plasmonic converter (PPC) to

focus the light into the active section, and the plasmonic waveguide. The active phase shifters are composed of a metal-insulator-metal waveguide with gold and BTO to form the plasmonic slot waveguide. To couple light from the SiN into the phase shifters, there are two stages. First, the signal is coupled to a BTO waveguide with a VDC from the SiN waveguide layer, see Fig. 1b. The length of the VDC in the C-band modulators, i.e., the MZ and the IQ modulator, is 80  $\mu\text{m}$  in length. For the O-band RT modulator, it is shortened to 40  $\mu\text{m}$  to achieve a shorter round-trip path for the light in the RT section. In Fig. 1b, the cross-section of the directional coupler is shown. The 800-nm-thick SiN waveguide is tapered from a width of 800 nm to 200 nm, whereas the ~200-nm-thick BTO waveguide located roughly 100 nm above the SiN, is tapered from a width of 150 nm to the single-mode waveguide of 800 nm in the C-band and 600 nm in the O-band. Cutback measurements in the C-band indicate that the propagation loss in the BTO is as low as 4.5 dB/cm and therefore has negligible losses for the short propagation distances of below 200  $\mu\text{m}$ . The transition loss of the VDC is 0.14 dB/transition determined from cutback measurements. In the PPC, light is focused into the plasmonic slot by tapering the BTO waveguide and bringing the metal closer until it touches the BTO to form the plasmonic slot, see Fig. 1c. The working principle of this plasmonic converter is described in our previous work and 3D finite-element (FEM) simulations indicate losses below 1 dB<sup>12</sup>. The measured losses are discussed in



the sections below. With the routing done in SiN, this phase shifter can be placed on top of more complicated structures to form different types of modulators. In the following, we discuss the experimental results of three modulator types: the C-band MZ, the C-band IQ, and the O-band resonant RT modulators.

### C-Band MZ modulator

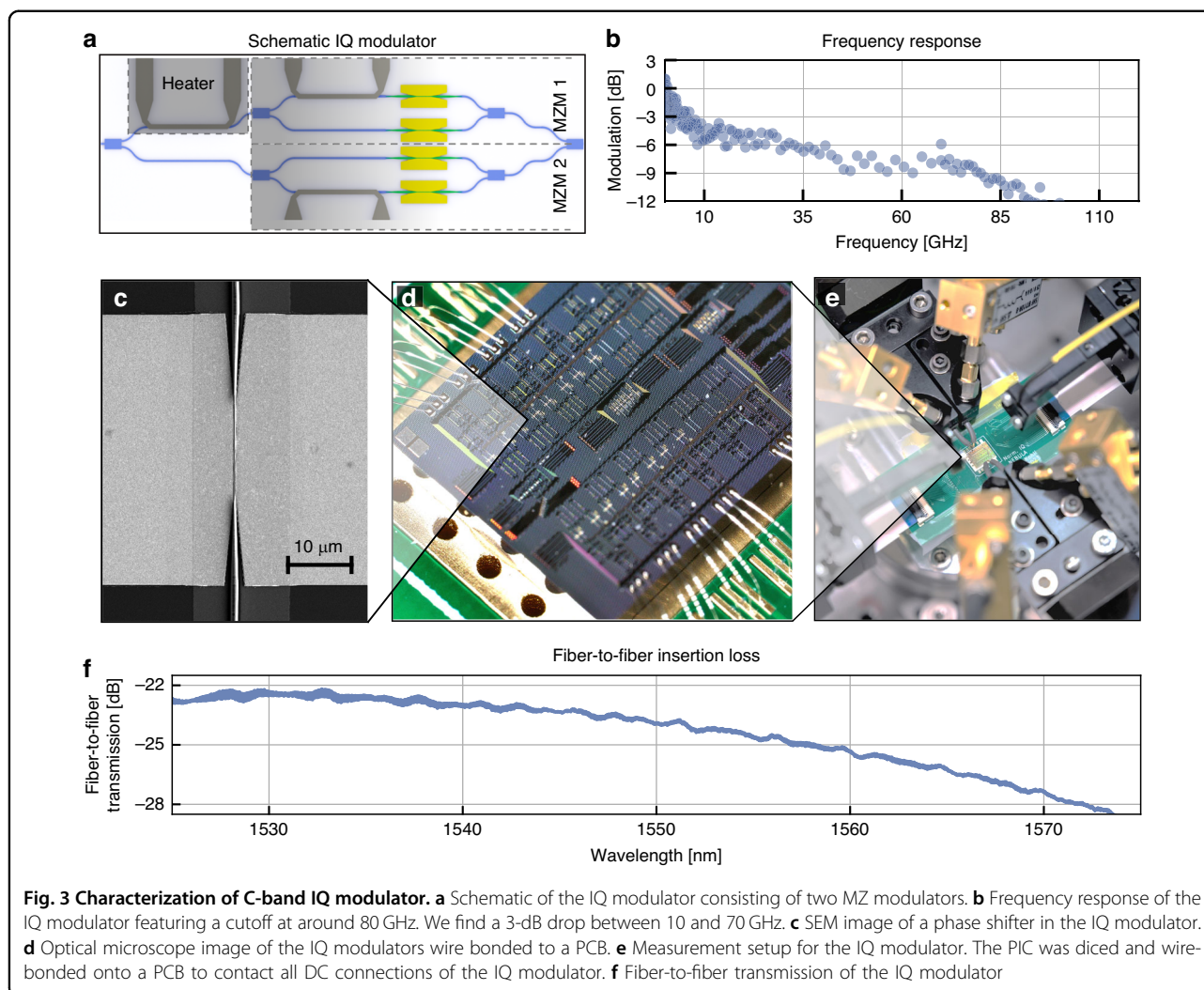
A schematic overview of the C-Band MZ modulator is shown in Fig. 2a. Light is first split into two arms with multi-mode interferometers in SiN. It is then coupled to the plasmonic phase-shifter sections and mapped back to waveguides where they are recombined in a multi-mode interferometer coupler (MMI). Figure 2b shows an optical microscope image of the fabricated device. The plasmonic phase-shifter section is 150 nm wide and 15  $\mu\text{m}$  long. The photonic-to-plasmonic converter is 15  $\mu\text{m}$  long. The fiber-to-fiber insertion losses are shown in Fig. 2c. In the current fabrication run, we found insertion losses (ILs) of  $-20.3$  dB at 1550 nm. Through cutback measurements, we found grating coupler losses of 2.8 dB per coupler, plasmonic propagation losses of 0.5 dB/ $\mu\text{m}$  in the 150-nm-wide slot, and 3.5 dB loss per photonic-to-plasmonic coupler. However, simulations and reference measurements indicate that the fiber-to-fiber losses can be ideally as low as 8.1 dB. These lower losses can be split onto 5 dB of losses in the plasmonic section (0.33 dB/ $\mu\text{m}$  as derived from measured material properties), 1 dB per PPC (3D FEM simulations, see ref. <sup>12</sup>), 0.1 dB per VDC transition for a total of 0.2 dB, and 0.44 dB per grating coupler with metallic mirror, see ref. <sup>56</sup>. There is thus room for fabrication improvement. Particularly, the PPC

show much higher losses than anticipated due to fabrication issues.

We measure a  $V_{\pi}$  of 3.6 V in the phase shifter or 1.8 V in the Mach-Zehnder configuration in push-pull configuration at DC. The frequency response of the phase shifters in the MZ modulator from 10 MHz to 110 GHz is shown in Fig. 2d. We find a drop-off between the MHz and the lower GHz ranges, leading to a  $V_{\pi}$  of 6.4 V at 40 GHz. We extract an effective Pockels effect of  $\sim 180$  pm/V at 40 GHz by comparing measured and simulated  $V_{\pi}$ . The drop is due to the frequency dependence of the Pockels effect in BTO and can be directly observed in a plasmonic configuration<sup>12,48</sup>. The response flattens after the initial drop and is followed by a small resonance around 75 GHz. We attribute this resonance to an LC peaking due to parasitic inductances of the prober set-up and device. The frequency response drops off around 110 GHz. The drop-off can be explained by an RC limit. This occurs due to the capacitance of the modulator and the 50 Ohm source. We expect improvements in the  $V_{\pi}$  and bandwidth with further optimizations of the device cross section and fabrication. Nevertheless, the BTO plasmonic MZ modulator reaches 110 GHz with a 3-dB drop-off between 10 GHz and 110 GHz, which suffices for highest symbol rates of 256 Gbd. Therefore, this modulator is more than capable of being employed in the next generations of Tbit/s links.

### C-Band IQ modulator

The schematic of the IQ modulator can be seen in Fig. 3a. It is composed of two parallel MZ modulators constituting the in-phase and quadrature phase modulators. A third

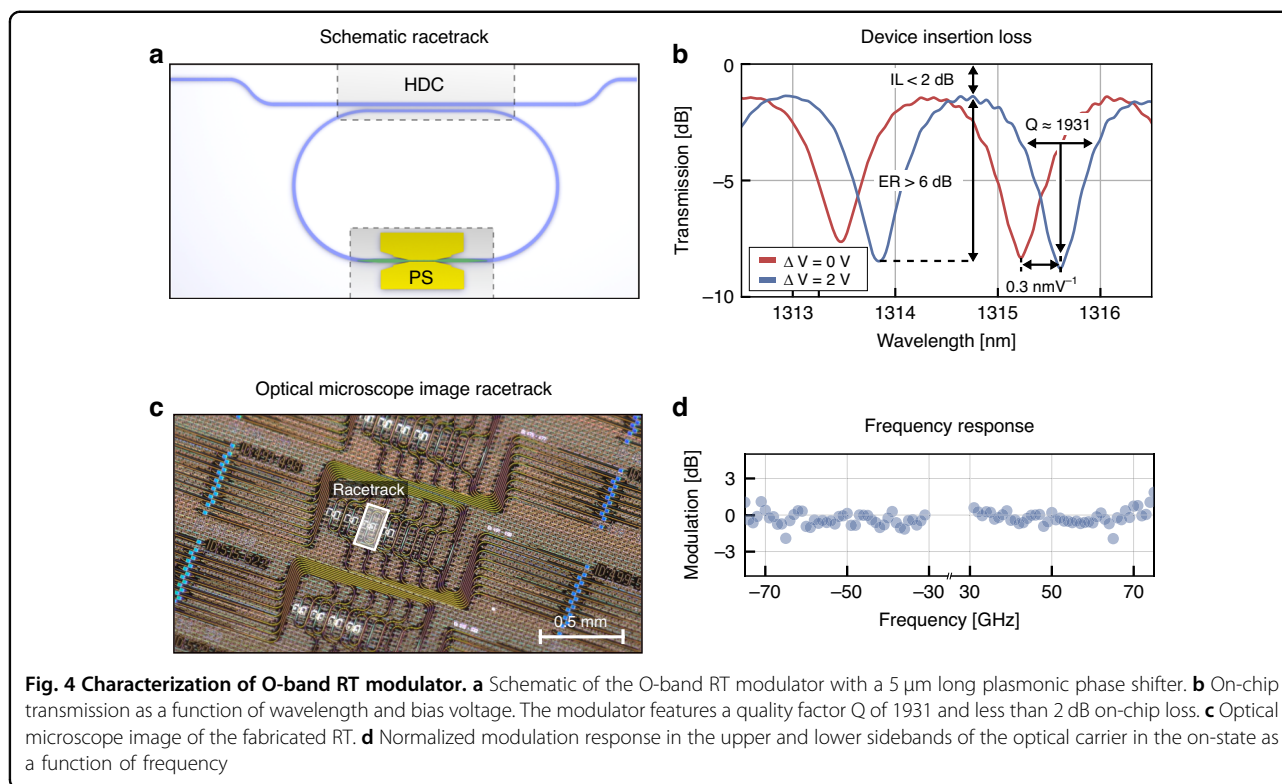


platinum heater is added to set the phase difference between the in-phase and quadrature signals. The footprint of a single IQ modulator is  $0.75 \times 2.15 \text{ mm}^2$ , dominated by the footprint of the three heaters ( $\sim 400 \times 150 \mu\text{m}^2$ ). The plasmonic sections in this IQ modulator are  $17.5 \mu\text{m}$  in length and  $100 \text{ nm}$  wide. Figure 3d shows an optical microscope image of the chip containing the IQ modulators. The diced PIC was placed on a PCB. Wire bonds connect the PIC to the PCB to contact the IQ modulators with the DC current sources for the heaters.

The fiber-to-fiber insertion loss of the IQ modulator is shown in Fig. 3f. The modulator features a total insertion loss of  $22.5 \text{ dB}$  at  $1530 \text{ nm}$  and  $23.9 \text{ dB}$  at  $1550 \text{ nm}$ . Through cutback measurements, we attribute  $\sim 2.75 \text{ dB}$  to the grating couplers,  $12.25 \text{ dB}$  to plasmonic losses in the active section ( $\sim 0.7 \text{ dB}/\mu\text{m}$ ) in the  $100 \text{ nm}$  wide plasmonic section and  $\sim 3 \text{ dB}$  per photonic-to-plasmonic coupler. Simulations indicate that the losses can be reduced to  $\sim 12 \text{ dB}$  fiber-to-fiber IL in this configuration. This

includes higher losses due to the narrower slot and longer length in comparison to the MZ modulator.

The electro-optic response was measured by applying a sinusoidal signal to the phase shifters in the IQ modulator. Figure 3b shows the electro-optic modulation as a function of frequency. We measure the characteristic drop between MHz and GHz, similarly to the MZ modulator. However, in the IQ modulator, the higher capacitance, due to a longer modulator and a smaller plasmonic gap, limits the bandwidth. The frequency response starts to drop at  $\sim 70 \text{ GHz}$ . We measure a  $V_\pi$  of  $4 \text{ V}$  in the phase-shifter or  $2 \text{ V}$  in the Mach-Zehnder configuration at DC voltages. The increased  $V_\pi$  in comparison to the MZ modulator could potentially arise from surface effects or dead layers in the BTO due to etching<sup>53</sup>, since the longer length and smaller width of the modulator should result in a lower  $V_\pi$ . Additionally, the bandwidth limitations further suggest that wider slots are preferable.



### O-Band RT modulator

The O-band RT modulator consists of a silicon nitride bus waveguide with a horizontal directional coupler (HDC) to a RT containing a plasmonic phase shifter, see Fig. 4a. Light is coupled from the bus waveguide into the RT. There is constructive or destructive interference between the light in the bus waveguide and the light from the RT. This is dependent on the phase difference accumulated through one round trip. Thus, there are transmission maxima and minima depending on the wavelength. With a phase shifter, the optical path length can be modulated within the RT, changing the spectral position of the minima, respective maxima. Figure 4b depicts the normalized on-chip transmission as a function of wavelength for two different voltages. The red and blue curves have different voltages applied with a  $\Delta V = 2\text{ V}$ . We find fiber-to-fiber transmission loss of  $-9.4\text{ dB}$  in the center of the O-band at 1310–1315 nm. Measurements of reference waveguides show on-chip device losses of less than 2 dB. The quality factor of the RT modulator is measured to be  $Q = 1931$  with an extinction ratio of more than 6 dB. The free spectral range is measured to be 1.79 nm. By applying a DC voltage to the phase shifter after fully poling the BTO, we measure a tuning efficiency of  $0.3\text{ nm/V}$ . This corresponds to a  $V_{\pi}$  of 3 V at DC. The frequency response of the modulator in the through-state is shown in Fig. 4d. Typically, resonant based modulators suffer from temperature sensitivity. Plasmonic racetrack

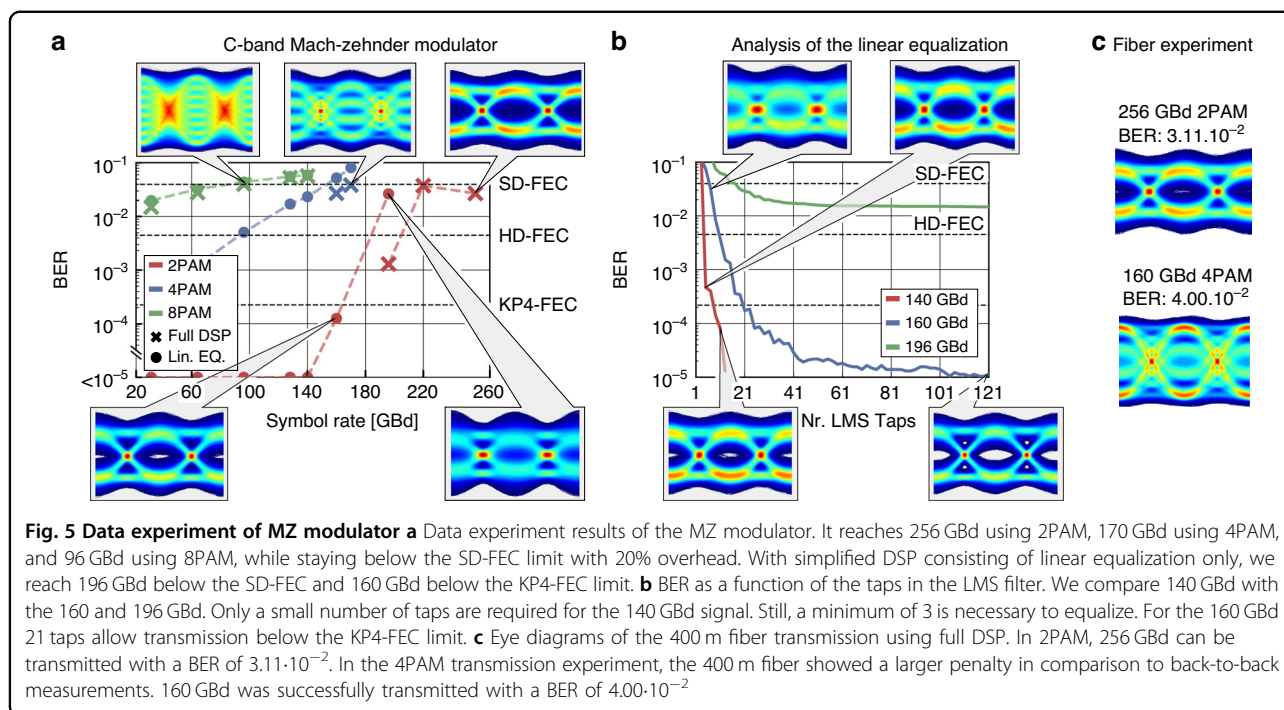
modulators, however, have shown an improved temperature sensitivity over silicon microring modulators<sup>61</sup>. Furthermore, the combination of plasmonics with BTO has shown stable modulation up to  $110^{\circ}\text{C}$  in a MZ configuration<sup>53</sup>. A similar temperature sensitivity is expected with this approach due to the small quality factor and small dimensions of the RT modulator.

## Discussion

### Performance in data experiments

The high-speed performance of the modulator is tested with data experiments in the C- and in the O-band for long- and short-haul applications.

The C-band MZ modulator operates at symbol rates up to 256 GBd. The measurement setup and DSP chain to achieve this high performance are described in the methods section. The bit-error ratio (BER) as a function of the transmitted symbol rate is shown in Fig. 5a. We reach a maximum symbol rate of 256 GBd using 2PAM with a BER of  $2.67 \cdot 10^{-2}$  with the full DSP consisting of linear and nonlinear equalization. This BER is below the soft-decision forward error correction (SD-FEC) limit with 20% overhead of  $4.0 \cdot 10^{-2}$ , see ref. <sup>62</sup>. For symbol rates up to 196 GBd, the BER is below the hard-decision FEC (HD-FEC) limit of  $3.8 \cdot 10^{-3}$ , see ref. <sup>63</sup>. The results of higher order modulation formats are shown in Fig. 5a in purple and light blue. We achieve a symbol rate of 170 GBd using 4PAM for a BER of  $3.75 \cdot 10^{-2}$ .



This corresponds to a maximum line rate with the MZ modulator of 340 Gbit/s. In the case of the 8PAM transmission experiment, 96 GBd is transmitted with a BER of  $3.98 \times 10^{-2}$ .

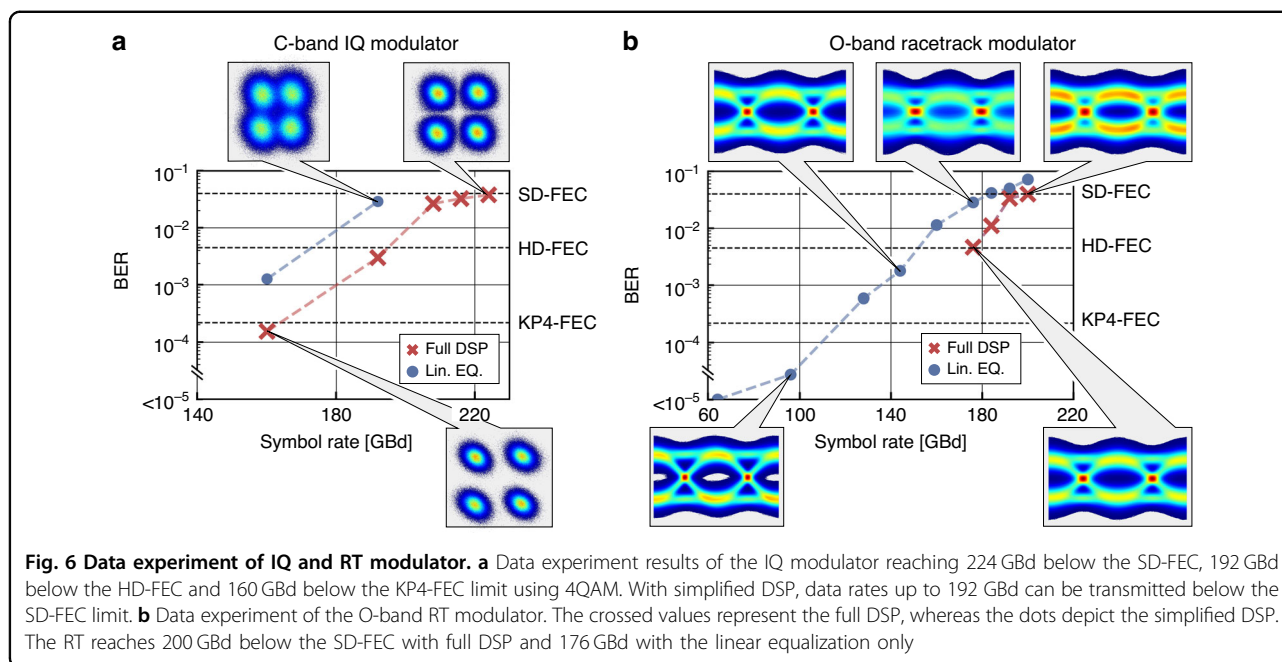
Furthermore, the modulator is tested in a fiber-transmission experiment with 400 m fiber length. The eye diagrams of these experiments are shown in Fig. 5c. There is only a small degradation when compared against the back-to-back eye diagrams. In detail, using 2PAM, 256 GBd was transmitted with a BER of  $3.10 \cdot 10^{-2}$ , while we transmitted 4PAM 160 GBd with a BER of  $4.00 \cdot 10^{-2}$ . We estimate the capacitance of the modulator to be  $\sim 30$  fF from the frequency response, which leads to an energy consumption of  $\sim 10$  fJ/bit in the MZ modulator.

The experiments are typically conducted with a full DSP consisting of linear and nonlinear equalization. However, certain applications require simpler complexity, e.g. number of multiplications in the data analysis. This is especially relevant for low-cost and energy-efficient IM/DD links. We thus further analyze the modulators by employing only linear equalization in the DSP chain, specifically with a timing recovery and a feed-forward equalization (FFE) with 21 taps in the IM/DD links. We demonstrate that the BTO-on-SiN modulators can offer up to 196 GBd even in this simpler setting, see Fig. 5a. For symbol rates up to 160 GBd, the BER is below the KP4-FEC limit. Only for higher symbol rates, nonlinear equalization is necessary to compensate for non-idealities in the electrical path. To analyze FFE's performance with the MZ modulator, the BER of different 2PAM signals is

plotted as a function of the number of taps in the FFE in Fig. 5b. With an FFE of less than 10 taps, the MZ modulator can transmit data below the KP4-FEC limit for symbol rates up to 140 GBd. With the 160 GBd signal, the KP4-FEC limit is achieved with only 21 taps.

With the more sophisticated C-band IQ modulator we show 224 GBd with a BER of  $3.79 \cdot 10^{-2}$  transmission with a coherent setup, see Methods. Figure 6a shows the data experiment and the received constellation diagrams of the C-band IQ modulator. The transmitted 224 GBd in 4QAM with a total line rate of 448 Gbit/s below the SD-FEC limit marks the highest data rate achieved both with BTO as active material on any substrate and with any nonlinear materials on silicon nitride. Similarly to the MZ modulator, simplified DSP with linear equalization only can be employed for symbol rates up to 192 GBd staying below the SD-FEC limit and up to 160 GBd below the HD-FEC limit. Full DSP can be used up to 160 GBd to remain below the KP4-FEC limit.

The resonant RT modulator was operated with 200 GBd in the O-band with a low 2 dB device insertion loss. The results of the data transmission experiment are shown in Fig. 6b. The modulator reaches 200 GBd using 2PAM with a BER of  $3.10 \cdot 10^{-2}$ . For symbol rates below 180 GBd, the transmitted signal has a BER below the HD-FEC limit. The same simplified DSP as for the MZ modulator can be employed up to 176 GBd. For rates up to 140 GBd, the BER is below the HD-FEC limit. Lower data rates in comparison to the C-band MZ modulator can be explained by three main reasons. First, the amplifier



employed in the O-band has a higher noise figure. Second, the photodetector is optimized for the C-band and has a lower responsivity in the O-band than those at 1550 nm. Thirdly, the optical bandwidth of the resonant modulator is lower than that of the MZ modulator due to the resonant effect. However, this could be solved by optimizing the design. For instance, resonant plasmonic devices with an organic electro-optic material operating in the C-band have already shown operation at 220 GBd employing RT modulators with bandwidths in excess of 100 GHz and presumably 200 GHz<sup>61</sup>. Similarly high numbers may be anticipated with BTO plasmonics by optimizing the plasmonic length, the coupling into the RT, and the total length of the cavity.

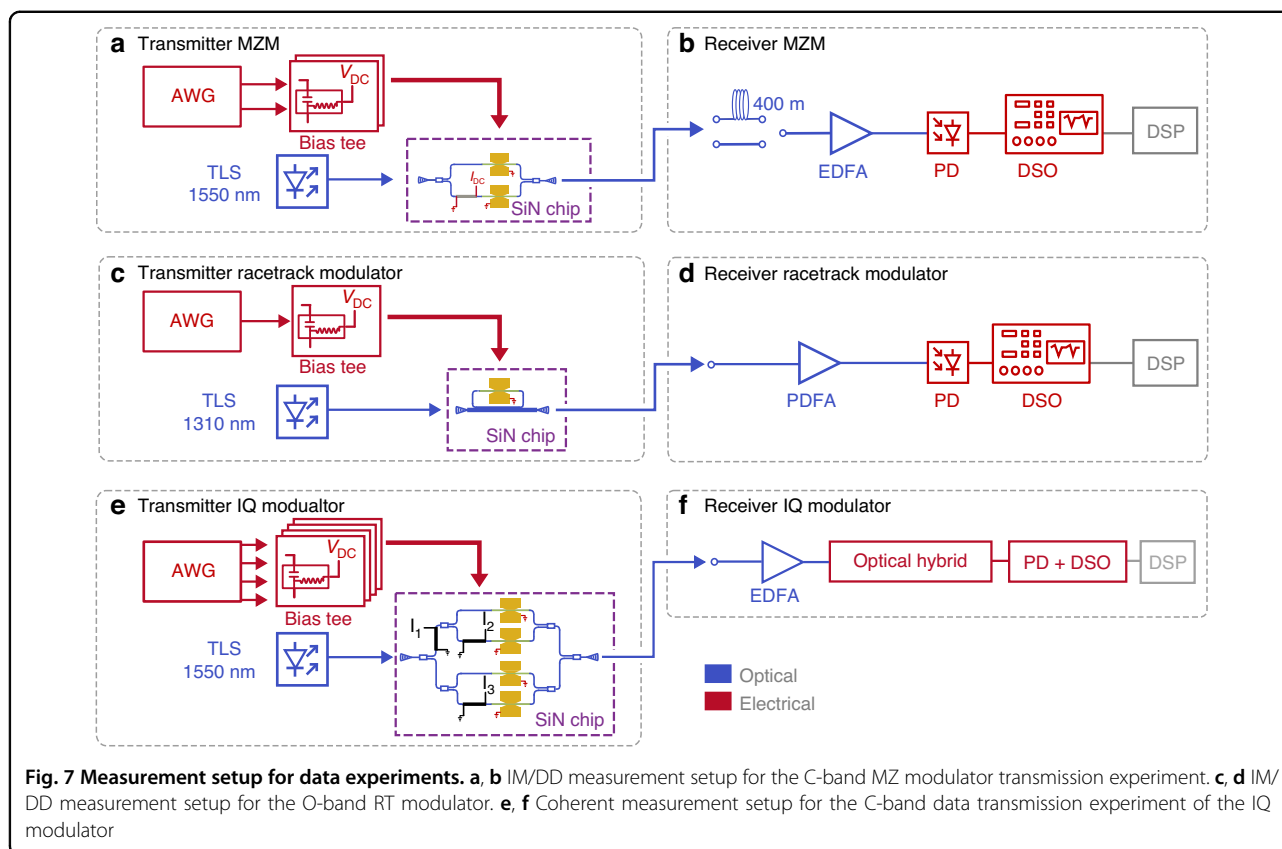
We demonstrate a high-speed BTO-on-SiN platform offering beyond 200 GBd data transmission using IM/DD in the C- and O-band and coherent communications in the C-band. All devices were fabricated on the same chip. The potential of this technology is demonstrated in multiple modulators. For instance, the C-band Mach-Zehnder modulator reaches 256 GBd in 2PAM and 170 GBd in 4PAM for a line rate of 340 Gbit/s. This modulator features a  $V_{\pi} = 1.8$  V at DC. The high-speed performance allows the employment of simplified DSP consisting only of timing recovery and linear equalization with 21 taps, while reaching 196 GBd. This allows a reduction of DSP complexity and therefore a reduction of energy consumption. We further demonstrate the first BTO-based IQ modulator and the first high-speed IQ modulator on the SiN platform. This modulator reaches 224 GBd 4QAM for a total of 448 Gbit/s line rate. Finally, the high-speed BTO plasmonic phase shifter can be

employed in an RT modulator. We demonstrate 200 GBd with an O-band BTO RT modulator featuring a 5  $\mu\text{m}$  long phase shifter and an on-chip loss of less than 2 dB. The same simplified DSP can be employed up to 176 GBd. We show a tuning efficiency of 0.3 nm/V with a quality factor of 1931. These demonstrations show that the BTO-on-SiN platform offers a solution for high-speed electro-optic modulators in short- and long-haul communications.

## Materials and methods

### Fabrication

The modulators in this work were all fabricated on the same chip. The SiN waveguides were produced in a photonic foundry on 8-inch wafers. An oxide cladding was used to cover the waveguides prior to being prepared for the wafer-scaled integration of the BTO active material. The modulators themselves were fabricated on the same die in a back-end-of-the-line (BEOL), chip-scale process on top of the BTO-on-SiN. The BTO was patterned using electron beam lithography. Afterwards, the material was etched to form the directional couplers and the BTO waveguides. The metallization to form the plasmonic slot was conducted with electron beam evaporation and patterns were defined with polymethylmethacrylate (PMMA). Amorphous silicon was deposited using plasma-enhanced chemical vapor deposition (PECVD). The gratings were etched locally using inductively coupled plasma reactive ion etching (ICP-RIE) and the silicon was removed selectively to the materials underneath without damaging the surface. In the next step, the chip was coated with SiO<sub>2</sub> deposited using PECVD as a cladding. For the heater structures,



further metallization steps needed to be added with crossings between metal layers in addition to SiN and BTO waveguides. Approximately  $1\ \mu\text{m}$  distance between the individual layers was used to lower loss and parasitic coupling. Connections between different metal layers in addition to openings for contacting were made by photolithography. These structures were etched using ICP-RIE. Finally, the chip was diced into different parts. The chip with the IQ modulators was bonded onto a PCB with a conductive glue and finally wire bonds were made to connect the PCB to the IQ modulators with the DC control voltages.

### Characterization

The cutback measurements were conducted using a tunable laser source in the C-band, respective O-band. An optical power meter was used to track the fiber insertion losses. Cutback measurements allowed an approximation of the losses in the individual components. The DC  $V_{\pi}$  was measured by applying a voltage directly from a small signal source to the modulator and tracking the optical output. Prior to sweeping the voltage, the BTO was fully poled. The high-speed electro-optic bandwidth measurements were conducted by applying a sinusoidal signal to the modulator. This signal was combined using a high-speed bias-tee. Two different methods to generate the

signal were used. For measurements up to 70 GHz, an RF source was directly used. The modulation sidebands were tracked with an optical spectrum analyzer. For the measurements from 70–110 GHz, an RF mixer was used to increase the frequency of the RF source. An overlap at 70 GHz allowed to match the signal of the generated signals. For calibration of the setup, the losses in the electrical path were measured by connecting it to an electrical spectrum analyzer. The losses of the probes were taken from the data sheet provided by the manufacturer.

### Data transmission experiment

The measurement setups of the data transmission experiments are shown in Fig. 7. In (a, b), the setup for the MZ modulator measurement is shown, in (c, d) for the RT modulator, and in (e, f) for the IQ modulator.

The MZ modulator was measured in an IM/DD setup. On the transmitter side, see Fig. 7a, a tunable laser in the C-band is coupled to the chip with  $\sim 20.3\ \text{dBm}$  input power to generate an optical carrier at  $\lambda = 1550\ \text{nm}$ . A periodically repeated signal is generated with an arbitrary waveform generator (AWG). These square-root-raised cosine shaped bit sequences were generated for symbol rates up to 256 Gbd. The signal is combined with a DC bias using a high-frequency bias-tee. The biasing is used

to pole the domains of the BTO and achieve best modulation efficiency. This voltage value was adapted to a value between 2 V and 3 V for all measurements in this work. On the receiver side, see Fig. 7b, the signal was amplified using an erbium-doped fiber amplifier (EDFA). We recorded the signal with a photodetector and a real-time digital sampling oscilloscope (DSO). We conducted two experiments with the MZ; one is optical back-to-back, and in the other the modulated signal is sent through a 400 m long fiber before the EDFA.

The measurement setup for the IQ modulator, see Fig. 7e, f is optimized for coherent communication. The MZ modulators were operated in push-pull. The carrier was set to  $\lambda = 1550$  nm with  $\sim 21$  dBm input power to the chip. On the receiver side, an optical hybrid consisting of two photodetectors with a local oscillator was employed after being amplified with an EDFA. The signal was then recorded with a DSO.

The measurement setup for the RT modulator, see Fig. 7c, is similar to the C-band MZ modulator. The laser is exchanged with a tunable laser in the O-band. The carrier was set to  $\lambda = 1315.7$  nm with an input power (in the fiber before the device) of  $\sim 13$  dBm. The EDFA was exchanged with a praseodymium-doped fiber amplifier (PDFA). A 70 GHz C-band photodetector was used, for which we expect a reduced responsivity in the O-band.

Two different types of DSP were employed for all measurements. The first type is linear equalization only. In the case of the MZ and the RT modulators, this simplified DSP consists of a timing recovery<sup>64</sup> and a feed forward equalizer (FFE) filter with 21 taps only. For the IQ modulator, an additional carrier recovery was conducted prior to the FFE. The full DSP was adapted for each modulation format and modulator individually. In the case of the MZ modulator, the full DSP consisted of a timing recovery with a T/2-spaced FFE similar to the simplified DSP. This FFE featured 151 taps. The nonlinear equalization was based on a 7-symbol pattern mapping (MAP). Finally, a second T-spaced FFE with 251 taps was applied. In the case of the 8PAM modulation format, the MAP was reduced to 5-symbols and the second FFE was increased to 1001 taps. In the case of the 4PAM, a third-order Volterra was added prior to the 7-symbol pattern mapping. Interestingly, full DSP for the 4PAM signal did not perform much better than the simplified DSP. By increasing the T-spaced FFE to 151 taps, 160 Gb/s in 4PAM was successfully transmitted below the SD-FEC limit. The full DSP of the RT modulator was identical to the DSP of the 2PAM signal with the MZ modulator. In the case of the IQ modulator, however, the DSP consisted of a carrier recovery, timing recovery, and a FFE with 251 taps. The nonlinear equalization consisted of a 7-symbol pattern mapping with a second FFE of 251 taps. For all modulators, an approximate driving voltage of

1.13 V<sub>pp</sub> was applied. This value was measured at 200 Gb/s with electrical back-to-back measurements. Losses of the electrical path were subtracted with values from the datasheets of the individual components at 50 GHz to include the approximate average losses as seen by the electrical signal.

#### Acknowledgements

This work was funded by the EC H2020 projects NEBULA (871658) and PlasmoniAC (871391). We thank the cleanroom operations team of the Binnig and Rohrer Nanotechnology Center (BRNC) for their help and support.

#### Author details

<sup>1</sup>ETH Zurich, Institute of Electromagnetic Fields, Zurich, Switzerland. <sup>2</sup>Ligentec SA, Ecublens, Switzerland. <sup>3</sup>Lumiphase AG, Stäfa, Switzerland

#### Author contributions

M.K. conceived the concept, designed, developed, and characterized the devices. J.L. conceived and supervised, and U.K. supervised this research. M.K., D.C., J.W., D.M., T.B., Y.H., A.M., Y.F., U.K., and J.L. gave conceptual suggestions. M.K., D.C., K.K., M.D., T.B., C.C., F.E., and Y.F. were involved in the development of fabrication methods and the fabrication of devices. The SiN wafers were fabricated by Ligentec with a lead by T.B. The growth and integration of the BTO was completed by Lumiphase with a lead by C.C. and F.E. M.K., D.C., J.W., D.M., and A.M. contributed to methodology and experiments. Data experiments were conducted by M.K., L.K. T.B., and Y.H. The original draft was written by M.K., while all authors were involved in the review and editing process.

#### Data availability

The data that support the findings of this study are available from the corresponding authors on reasonable request.

#### Conflict of interest

F.E. and C.C. are involved in commercializing the barium titanate photonic technologies at Lumiphase AG.

**Supplementary information** The online version contains supplementary material available at <https://doi.org/10.1038/s41377-025-02116-1>.

Received: 14 August 2024 Revised: 14 October 2025 Accepted: 2 November 2025

Published online: 16 December 2025

#### References

1. Winzer, P. J. & Neilson, D. T. From scaling disparities to integrated parallelism: a decathlon for a decade. *J. Lightwave Technol.* **35**, 1099–1115 (2017).
2. PsiQuantum Team A manufacturable platform for photonic quantum computing. *Nature* **641**, 876–883 (2025).
3. Eltes, F. et al. An integrated optical modulator operating at cryogenic temperatures. *Nat. Mater.* **19**, 1164–1168 (2020).
4. Lecocq, F. et al. Control and readout of a superconducting qubit using a photonic link. *Nature* **591**, 575–579 (2021).
5. Youssefi, A. et al. A cryogenic electro-optic interconnect for superconducting devices. *Nat. Electron.* **4**, 326–332 (2021).
6. Bisang, D. et al. Plasmonic modulators in cryogenic environment featuring bandwidths in excess of 100 GHz and reduced plasmonic losses. *ACS Photonics* **11**, 2691–2699, <https://doi.org/10.1021/acsp Photonics.4c00507> (2024).
7. Lee, B. G. et al. Beyond CPO: a motivation and approach for bringing optics onto the silicon interposer. *J. Lightwave Technol.* **41**, 1152–1162 (2023).
8. Marpaung, D., Yao, J. P. & Capmany, J. Integrated microwave photonics. *Nat. Photonics* **13**, 80–90 (2019).
9. Burla, M. et al. 500 GHz plasmonic Mach-Zehnder modulator enabling sub-THz microwave photonics. *APL Photonics* **4**, 056106 (2019).
10. Ying, Z. F. et al. Electronic-photonic arithmetic logic unit for high-speed computing. *Nat. Commun.* **11**, 2154 (2020).

11. Sun, C. et al. Single-chip microprocessor that communicates directly using light. *Nature* **528**, 534–538 (2015).
12. Kohli, M. et al. Plasmonic ferroelectric modulator monolithically integrated on SiN for 216 Gbd data transmission. *J. Lightwave Technol.* **41**, 3825–3831, <https://doi.org/10.1109/JLT.2023.3260064> (2023).
13. Kulmer, L. et al. Single carrier net 400 Gbit/s IM/DD over 400 m fiber enabled by plasmonic Mach-zehnder modulator. In *Proceedings of the 2024 Optical Fiber Communications Conference and Exhibition (OFC)*, 1–3 (IEEE, 2024).
14. Mardoyan, H. et al. First 260-Gbd single-carrier coherent transmission over 100 km distance based on novel arbitrary waveform generator and thin-film lithium niobate IQ modulator. In *Proceedings of the 2022 European Conference on Optical Communication (ECOC)*, 1–4 (IEEE, 2022).
15. Kulmer, L. et al. 256 Gbd single-carrier transmission over 100km SSMF by a plasmonic IQ modulator. In *Proceedings of the 49th European Conference on Optical Communications (ECOC 2023)*, 1449–1452 (IEEE, 2023).
16. Berikaa, E. et al. Silicon photonic single-segment IQ modulator for net 1 Tbps/ $\lambda$  transmission using all-electronic equalization. *J. Lightwave Technol.* **41**, 1192–1199 (2023).
17. Xu, M. Y. et al. Dual-polarization thin-film lithium niobate in-phase quadrature modulators for terabit-per-second transmission. *Optica* **9**, 61–62 (2022).
18. Wakita, H. et al. 100-GHz-bandwidth InP-based on-board coherent Tx front-end enabling 2-Tb/s/ $\lambda$  optical transmission. In *Proceedings of the 2024 Optical Fiber Communications Conference and Exhibition (OFC)*, 1–3 (IEEE, 2024).
19. Zhou, X., Urata, R. & Liu, H. Beyond 1 Tb/s intra-data center interconnect technology: IM-DD OR coherent?. *J. Lightwave Technol.* **38**, 475–484 (2020).
20. Ozolins, O. et al. Optical amplification-free 310/256 gbaud OOK, 197/145 gbaud PAM4, and 160/116 gbaud PAM6 EML/DML-based data center links. In *Proceedings of the Optical Fiber Communication Conference (OFC) 2023*. (Optica Publishing Group, 2023) <https://doi.org/10.1364/OFC.2023.Th4B.2>.
21. Berikaa, E. et al. TFLN MZMs and next-gen DACs: enabling beyond 400 Gbps IMDD O-band and C-band transmission. *IEEE Photonics Technol. Lett.* **35**, 850–853 (2023).
22. St-Arnauld, C. et al. Net 1.6 Tbps (4x400Gbps/ $\lambda$ ) O-band IM/DD transmission over 2 km using uncooled DFB lasers on the LAN-WDM grid and Sub-1V drive TFLN modulators. In *Proceedings of the 2024 Optical Fiber Communications Conference and Exhibition (OFC)*, 1–3 (IEEE, 2024).
23. Ostrovskis, A. et al. Heterogenous InP electro-absorption modulator with Si waveguides for beyond 200 Gbps/ $\lambda$  optical interconnects. In *Proceedings of the 2024 Optical Fiber Communications Conference and Exhibition (OFC)*, 1–3 (IEEE, 2024), 1–3.
24. Puckett, M. W. et al. 422 million intrinsic quality factor planar integrated all-waveguide resonator with sub-MHz linewidth. *Nat. Commun.* **12**, 934 (2021).
25. Liu, J. Q. et al. High-yield, wafer-scale fabrication of ultralow-loss, dispersion-engineered silicon nitride photonic circuits. *Nat. Commun.* **12**, 2236 (2021).
26. Wilmart, Q. et al. A versatile silicon-silicon nitride photonics platform for enhanced functionalities and applications. *Appl. Sci.* **9**, 255 (2019).
27. Heideman, R. et al. Large-scale integrated optics using TriPLeX waveguide technology: from UV to IR. In *Proceedings of SPIE 7221, Photonics Packaging, Integration, and Interconnects IX* (SPIE, 2009).
28. Gyger, F. et al. Observation of stimulated Brillouin scattering in silicon nitride integrated waveguides. *Phys. Rev. Lett.* **124**, 013902 (2020).
29. Kim, S. et al. Dispersion engineering and frequency comb generation in thin silicon nitride concentric microresonators. *Nat. Commun.* **8**, 372 (2017).
30. Raja, A. S. et al. Electrically pumped photonic integrated soliton microcomb. *Nat. Commun.* **10**, 680 (2019).
31. Liu, Y. et al. A photonic integrated circuit-based erbium-doped amplifier. *Science* **376**, 1309–1313 (2022).
32. Mahmudlu, H. et al. Fully on-chip photonic turnkey quantum source for entangled qubit/qudit state generation. *Nat. Photonics* **17**, 518–524 (2023).
33. Gundavarapu, S. et al. Sub-hertz fundamental linewidth photonic integrated Brillouin laser. *Nat. Photonics* **13**, 60–67 (2019).
34. Jin, W. et al. Hertz-linewidth semiconductor lasers using CMOS-ready ultra-high-Q microresonators. *Nat. Photonics* **15**, 346–353 (2021).
35. Thomaschewski, M. & Bozhevolnyi, S. I. Pockels modulation in integrated nanophotonics. *Appl. Phys. Rev.* **9**, 021311 (2022).
36. Zhu, X. R. et al. Twenty-nine million intrinsic Q-factor monolithic microresonators on thin-film lithium niobate. *Photonics Res.* **12**, A63–A68 (2024).
37. Snigirev, V. et al. Ultrafast tunable lasers using lithium niobate integrated photonics. *Nature* **615**, 411–417 (2023).
38. Zhang, M. et al. Broadband electro-optic frequency comb generation in a lithium niobate microring resonator. *Nature* **568**, 373–377 (2019).
39. Alexander, K. et al. Nanophotonic Pockels modulators on a silicon nitride platform. *Nat. Commun.* **9**, 3444 (2018).
40. Zhang, P. et al. High-speed electro-optic modulator based on silicon nitride loaded lithium niobate on an insulator platform. *Opt. Lett.* **46**, 5986–5989 (2021).
41. Jiang, Y. H. et al. Monolithic photonic integrated circuit based on silicon nitride and lithium niobate on insulator hybrid platform. *Adv. Photonics Res.* **3**, 2200121 (2022).
42. Ruan, Z. L. et al. High-performance electro-optic modulator on silicon nitride platform with heterogeneous integration of lithium niobate. *Laser Photonics Rev.* **17**, 2200327 (2023).
43. Vanackere, T. et al. Heterogeneous integration of a high-speed lithium niobate modulator on silicon nitride using micro-transfer printing. *APL Photonics* **8**, 086102 (2023).
44. Valdez, F., Mere, V. & Mookherjee, S. 100 GHz bandwidth, 1 volt integrated electro-optic Mach-Zehnder modulator at near-IR wavelengths. *Optica* **10**, 578 (2023).
45. Churaev, M. et al. A heterogeneously integrated lithium niobate-on-silicon nitride photonic platform. *Nat. Commun.* **14**, 3499 (2023).
46. Ortmann, J. E. et al. Ultra-low-power tuning in hybrid barium Titanate-silicon nitride electro-optic devices on silicon. *ACS Photonics* **6**, 2677–2684 (2019).
47. Abel, S. et al. Large Pockels effect in micro- and nanostructured barium titanate integrated on silicon. *Nat. Mater.* **18**, 42–47 (2019).
48. Winiger, J. et al. PLD epitaxial thin-film BaTiO<sub>3</sub> on MgO — dielectric and electro-optic properties. *Adv. Mater. Interfaces* **11**, 2300665 (2024).
49. Dong, Z. M. et al. Monolithic barium Titanate modulators on silicon-on-insulator substrates. *ACS Photonics* **10**, 4367–4376 (2023).
50. Posadas, A. B. et al. RF-sputtered Z-cut electro-optic barium Titanate modulator on silicon photonic platform. *J. Appl. Phys.* **134**, 073101 (2023).
51. Zgonik, M. et al. Dielectric, elastic, piezoelectric, electro-optic, and elasto-optic tensors of BaTiO<sub>3</sub> crystals. *Phys. Rev. B* **50**, 5941–5949 (1994).
52. Eltes, F. et al. A BaTiO<sub>3</sub>-based electro-optic pockels modulator monolithically integrated on an advanced silicon photonics platform. *J. Lightwave Technol.* **37**, 1456–1462 (2019).
53. Messner, A. et al. Plasmonic ferroelectric modulators. *J. Lightwave Technol.* **37**, 281–290 (2019).
54. Kohli, M. et al. 256 Gbd barium-titanate-on-SiN mach-zehnder modulator. In *Proceedings of the 2024 Optical Fiber Communications Conference and Exhibition (OFC)*, 1–3 (IEEE, 2024).
55. Kohli, M. et al. Barium Titanate racetrack modulator on silicon nitride for 200 Gbd data communication in the O-band. In *Proceedings of the 2024 Conference on Lasers and Electro-Optics (CLEO)*, 1–3 (IEEE, 2024).
56. Kohli, M. et al. C- and O-band dual-polarization fiber-to-chip grating couplers for silicon nitride photonics. *ACS Photonics* **10**, 3366–3373 (2023).
57. Dong, P. et al. Thermally tunable silicon racetrack resonators with ultralow tuning power. *Opt. Express* **18**, 20298–20304 (2010).
58. Pfeifle, J. et al. Silicon-organic hybrid phase shifter based on a slot waveguide with a liquid-crystal cladding. *Opt. Express* **20**, 15359–15376 (2012).
59. Hattori, A. et al. Integrated visible-light polarization rotators and splitters for atomic quantum systems. *Opt. Lett.* **49**, 1794–1797 (2024).
60. van Iseghem, L. et al. Low power optical phase shifter using liquid crystal actuation on a silicon photonics platform. *Optical Mater. Express* **12**, 2181–2198 (2022).
61. Eppenberger, M. et al. Resonant plasmonic micro-racetrack modulators with high bandwidth and high temperature tolerance. *Nat. Photonics* **17**, 360–367 (2023).
62. Schuh, K. et al. Single carrier 1.2 Tbit/s transmission over 300 km with PM-64 QAM at 100 GBaud. In *Proceedings of the 2017 Optical Fiber Communications Conference and Exhibition (OFC)*, 1–3 (IEEE, 2017).
63. El-Fiky, E. et al. First demonstration of a 400 Gb/s 4 $\lambda$  CWDM TOSA for data-center optical interconnects. *Opt. Express* **26**, 19742–19749 (2018).
64. Josten, A. et al. Modified Godard timing recovery for Non Integer oversampling receivers. *Appl. Sci.* **7**, 655 (2017).